Electronic Structure of Two-Dimensional Lead(II) Iodide Perovskites: An Experimental and Theoretical Study

Phuyala, D.; Safdari, M.; Pazoki, M.; Liu, P.; Philippe, B.; Kvashnina, K. O.; Karis, O.; Butorin, S. M.; Rensmo, H.; Edvinsson, T.; Kloob, L.; Gardner, J. M.;

Originally published:

August 2018

Chemistry of Materials 30(2018)15, 4959-4967

DOI: https://doi.org/10.1021/acs.chemmater.8b00909

Effect on the Electronic Structure of Two Dimensional Lead (II) Iodide Perovskites by Inter-Layer Distance Tuning

Journal:	*Chemistry of Materials*
Manuscript ID	Draft
Manuscript Type:	Article
Date Submitted by the Author:	n/a
Complete List of Authors:	Phuyal, Dibya; Uppsala University, Department of Physics and Astronomy Safdari, Majid; KTH Royal Institute of Technology, Department of Chemistry Pazoki, Meysam; Uppsala University, Department of Engineering Sciences - Solid State Physics Liu, Peng; KTH Royal Institute of Technology, Department of Chemistry Philippe, Bertrand; Uppsala University, Department of Physics and Astronomy Kvashnina, Kristina; ESRF; Helmholtz-Zentrum Dresden-Rossendorf, Institute of Resource Ecology Karis, Olof; Uppsala University, Department of Physics and Astronomy Butorin, Sergei; Uppsala University, Department of Physics and Astronomy Rensmo, Håkan; Uppsala University, Department of Physics and Astronomy Edvinsson, Tomas; Uppsala University, Department of Engineering Sciences - Solid State Physics Kloo, Lars; KTH Royal Institute of Technology, Department of Chemistry Gardner, James; KTH Royal Institute of Technology, Department of Chemistry

Effect on the Electronic Structure of Two Dimensional Lead (II) Iodide Perovskites by Inter-Layer Distance Tuning

Dibya Phuyal[a‡], Majid Safdari[b‡], Meysam Pazoki[c], Peng Liu[b], Bertrand Philippe[a], Kristina O. Kvashnina[d, e], Olof Karis[a], Sergei M. Butorin[a], Håkan Rensmo[*a], Tomas Edvinsson[c], Lars Kloo[b], and James M. Gardner[*b]

[a] Dept. of Physics and Astronomy, Uppsala Univ., Box 516, SE-75121, Uppsala, Sweden.

[b] Division of Applied Physical Chemistry, Department of Chemistry, KTH Royal Institute of Technology, SE-100 44, Stockholm, Sweden. E-mail: jgardner@kth.se.

[c] Department of Engineering Sciences, Solid State Physics, Ångström Laboratory, Uppsala University, Uppsala, Sweden.

[d] Rossendorf Beamline at ESRF – The European Synchrotron, CS40220, 38043 Grenoble Cedex 9, France

[e] Helmholtz Zentrum Dresden-Rossendorf (HZDR), Institute of Resource Ecology, PO Box 510119, 01314 Dresden, Germany

KEYWORDS: halide perovskites, layered materials, dimensional tuning, x-ray spectroscopy, density functional theory

ABSTRACT: Layered two-dimensional (2D) hybrid organic-inorganic perovskites (HOP) are promising materials for light harvesting applications due to their chemical stability, wide flexibility in composition, and recent increases in photovoltaic power conversion efficiencies. Three 2D lead iodide perovskites were studied through various X-ray spectroscopic techniques to derive detailed electronic structures and band energetics profiles at a titania interface. Core-level and valence band photoelectron spectra of HOP were analyzed to resolve the electronic structure changes due to the reduced-dimensionality of inorganic layers. The results show orbital narrowing when comparing the HOP, the layered precursor PbI_2, and the conventional 3D $(CH_3NH_3)PbI_3$ such that different localizations of band edge states and narrow band states are unambiguously due to the decrease in dimensionality of the layered HOPs. Support from density functional theory (DFT) calculations provide further details on the interaction and bandgap variations of the electronic structure. We observed an interlayer distance dependent dispersion in the near band edge electronic states. The results show how tuning the interlayer distance between the inorganic layers affects the electronic properties and provides important design principles for control of the interlayer charge transport properties, such as the change in effective charge masses as a function of the organic cation length. The results of these findings can aid in establishing design principles for new, layered materials.

1. INTRODUCTION

Organic-inorganic lead halide perovskites have been investigated for over three decades[1, 2] but their application in solar cells dates back merely to 2009.[3] Since then, impressive improvements and breakthroughs have led to power conversion efficiencies beyond 22%.[4, 5] Improvements in solar cell architecture[6] and sample preparation processes[7-10] during the interceding years has led to the impressive efficiencies we have today. Despite remarkable efficiency improvements, there are major questions that need to be addressed regarding thermal and moisture instabilities of the most efficient perovskites that are still lead-based ($CH_3NH_3PbI_3$ and its derivatives) and their related problems with toxicity.[11-14] The chemical structure of $CH_3NH_3PbI_3$ and its derivatives consist of three-dimensional networks of corner-shared octahedral [PbI_6] units, which form a cavity that facilitates the intercalation of $CH_3NH_3^+$ (MA^+) or $NH_2CHNH_2^+$ (FA^+) cations.[11, 15] Substitution of $CH_3NH_3^+$ or $NH_2CHNH_2^+$ cations with molecules that have larger cationic radii results in lowering the network dimensionality to a two-dimensional (2D) layered structure. Layered perovskites have opened an impressive approach to the perovskite solar cells that are significantly more stable and have power conversion efficiencies now surpassing 12% for multilayered materials.[16-18] Later reports used the stabilizing concepts of these materials toward even more efficient devices[19] as well as larger device sizes that require durability standards.[20] In ongoing work, 2D materials are being used as dopants in 3D host materials or terminating phases as an alternative to a fully 2D layered structure.

Previously, we have investigated 2D perovskite materials with dialkylammonium cations [(dA)PbI_4] for use in solar cells; butyl-1,4-diammonium lead(II) iodide [(BdA)PbI_4], hexyl-1,6-diammonium lead(II) iodide [(HdA)PbI_4], and octyl-1,8-diammonium lead(II) iodide [(OdA)PbI_4].[21] Although (BdA)PbI_4 has a relatively high bandgap for a light absorption in a single-junction solar cell (2.37eV), it had the highest power conversion efficiency of the pure 2D perovskites (1.1%).[21] A preliminary attempt in device fabrication for 2D

perovskites is in a similar solar cell architecture to those based on the optimized configuration for $(CH_3NH_3)PbI_3$ solar cells.[21] However, to understand the mechanism for light absorption and electron transfer in 2D perovskite solar cells, it is imperative to learn more about their electronic structures. To probe these properties, we use x-ray spectroscopy to directly observe the occupied and unoccupied electronic levels in the material. We exploit the combination of hard X-ray photoelectron spectroscopy (HAXPES), high-resolution fluorescence detected X-ray absorption near edge structure (HERFD-XANES), and resonant inelastic X-ray scattering (RIXS) to draw a picture of the partial density of states (PDOS) for the valence and conduction band (VB, CB).[22] To support the experimental methods, density functional theory (DFT) is used to calculate the partial and total density of states as well as the band structure in the different inter-layered systems. The relation between the electronic structure and previously reported chemical structure[21] provides a comprehensive understanding for the future design of new, stable, layered 2D perovskites for solar cell applications.

The three 2D HOP structures analyzed in this study along with the 3D $MAPbI_3$ and PbI_2 consist of inorganic PbI_6 octahedra where the 2D structures consist of sheets separated by bilayers of alkylammonium cations that are largely held together through van der Waals interactions in between the alkyl chains.[21, 23] For $(dA)PbI_4$ materials, the formal electronic configurations of Pb $6s^26p^0$ and I $5s^25p^6$ are apparent from their oxidation states. At least in the case of $(CH_3NH_3)PbI_3$, this translates to the valence band edge that is largely formed from I *p* orbitals and the conduction band edge formed from the unoccupied Pb *p* orbitals.[24] The organic cations in the perovskite framework do not constitute a primary role in the states close to the valence and conduction band edges, but indirectly influence them by deforming the lattice and tuning of dimensionality. Here, utilizing element specific X-ray spectroscopic techniques, we provide a detailed survey of the electronic and chemical properties of these light-absorbing materials, as well as examine the relevance of these specific techniques in their application to 2D and 3D perovskites. By combining X-ray spectroscopy results with DFT calculations, an in-depth understanding of the electronic structure of these 2D perovskite materials is obtained.

2. EXPERIMENTAL AND COMPUTATION

2.1 HAXPES

HAXPES was carried out at BESSY II (Helmholtz Zentrum Berlin) at the KMC-1 beamline using the HIKE end-station.[25] A photon energy of 4000 eV was selected using a first-order light from a Si (311) double-crystal monochromator (Oxford-Danfysik), and the photoelectron kinetic energies (KE) were measured using a Scienta R4000 analyzer optimized for high kinetic energies. An X-ray grazing incidence angle of ~ 5° relative to the surface and normal emission to the electron analyzer was used. The base pressure in the analysis chamber was ~ 10^{-8} mbar. All spectra were energy calibrated versus the Fermi level, defined to be at zero binding energy, which was determined by measuring a gold foil in electric contact with the sample and setting the Au $4f_{7/2}$ core level peak to 84.0 eV. The spectral intensity is normalized to the maximum intensity if not stated otherwise. Quantitative ratios presented between different core levels were calculated from the experimental results after correcting the intensity by the photoionization cross sections for each element using database values.[26]

2.2 HERFD-XANES & RIXS

The HERFD-XANES and RIXS experiments were performed at beamline ID26 at the European Synchrotron Radiation Facility.[27] The incident energy was selected using the Si (311) reflection from a double Si crystal monochromator. The energy calibration was performed using the PbI_2 precursor. The HERFD-XANES (henceforth referred to XANES) spectra, as well as, the experimental procedure used to obtain them have been described previously.[28] XANES data at the I L_1 edge were recorded at the maximum of the $L\gamma_{2,3}$ emission line (h□□= 5065 eV). RIXS spectra were recorded at the excitation energy of the first maximum of iodine L_1 edge in the energy range of 5173-5196 eV with a step size of 0.2 eV. The emitted energy in XANES and RIXS was selected using the (331) reflection of three spherically bent Si crystal analyzers. The intensity was normalized to the incident flux measured using a photodiode. Samples were positioned at 45˚ to the beam. A helium-filled bag was used to reduce absorption of the fluorescence radiation between the sample and the spectrometer. The resolution of the monochromator and spectrometer is around 0.5 eV and 0.6 eV respectively. Measurements were carried out on multiple spots on the samples to assess radiation damages. No radiation damages could be detected within the acquisition time (5 min for HERFD and 25 min for RIXS) for the different spectra.

2.3 COMPUTATIONAL METHODS

All theoretical calculations were performed with Quantum Espresso package [29] according to previously reported procedure for lead perovskite[30-32]. In summary, the Perdew-Burke-Ernzerhof[33] exchange-correlation functional together with a plane wave basis set was implemented together with pseudopotentials. Our implemented non-spin-orbit coupling (SOC) scalar relativistic calculations based on generalized gradient approximation (GGA) has been shown to predict the band gap of the lead[34] and bismuth[35] perovskites where the good agreement between the theoretical and experimental data is partly due to error cancelation[34]; however, the amount of the error cancelation is different for lead and bismuth.[35] The starting configurations in the unit cells of the 2D-HOPs in the present study were based on experimental XRD data[36] and the lead 5*d*/ 6*s*/ 6*p*, the nitrogen 2*s*/2*p* , the iodide 5*s*/5*p* , and the carbon 2*s*/2*p* electrons were considered as valence electrons. All unit-cell vectors and atom coordinates were geometry relaxed to have a total force lower than 0.08 Ry/a.u. Cutoff energies for the plane wave function and the charge density were set to 45 and 450 Rydberg, respectively. Brillouin zone samplings were carried out on a 3x3x3 Monkhorst-Pack grid (MPG) during the relaxation procedure, a 4x4x4 MPG for the self-consistent procedures, and a 6x6x6 MPG for the non-self-consistent procedures. The Xcrysden package[37] was used for visualization of the charge densities.

3. RESULTS AND DISCUSSION

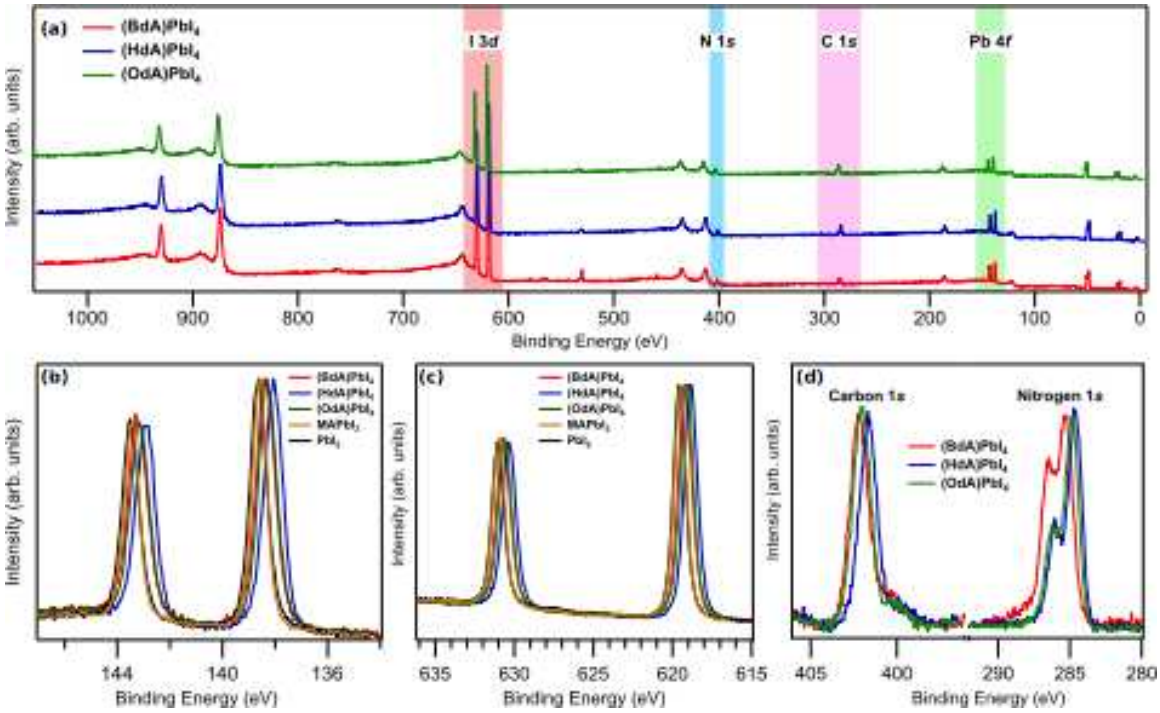

Figure 1. HAXPES measurements on the three 2D HOP and $MAPbI_3$ and PbI_2 measured at 4000 eV. (a) Overview spectrum of the three 2D HOP samples on a TiO_2/FTO substrate. The intensities are scaled *vs.* I 3*d* intensity and vertically offset for comparison, (b) Pb 4*f* core level peaks measured with photon energy of 4000 eV. The peaks are normalized to $4f_{7/2}$ intensity for comparison, (c) I 3*d* core level peaks, and (d) C 1*s* and N 1*s* core levels. Nitrogen spectra are normalized to maximum intensity and carbon spectra are normalized to Pb $4f_{7/2}$ intensity.

The HAXPES overview spectra of the various $(dA)PbI_4$ materials film deposited on top of a TiO_2/FTO substrate are shown in Figure 1a [dA is the organic di-cation: $[NH_3(CH_2)_XNH_3]^{2+}$; X = 4 (BdA), X = 6 (HdA), and X = 8 (OdA)]. As expected, the samples display carbon, nitrogen, iodine, and lead. The mesoporous TiO_2 substrate is perfectly covered as no titanium or oxygen peaks are detected, indicating thorough film coverage. An appropriate estimation of sample stoichiometry was made by measuring the I 4*d* and Pb 5*d* core level intensities (Figure S1). The estimation takes into account differential atomic subshell photoionization cross-sections. On the basis of these cross sections, we obtain experimental relative intensities that to a first approximation are in accordance with what is expected from the stoichiometry of $(BdA)PbI_4$, $(HdA)PbI_4$, and $(OdA)PbI_4$, (Table 1).

Table 1. Ratio of the recorded intensities from iodide and lead core levels as calculated from overview spectra. Experimental results are in accordance with the expected ratios from the chemical formula.

Sample	I/Pb	Formula
$(BdA)PbI_4$– $[NH_3(CH_2)_4NH_3]PbI_4$	3.82	4
$(HdA)PbI_4$– $[NH_3(CH_2)_6NH_3]PbI_4$	4.09	4
$(OdA)PbI_4$– $[NH_3(CH_2)_8NH_3]PbI_4$	3.85	4
$MAPbI_3$ – $(CH_3NH_3)PbI_3$	2.70	3
PbI_2	1.80	2

The experimental Pb 4*f* signals for the three samples along with PbI_2 are shown in Figure 1b. The spin-orbit splitting between Pb $4f_{7/2}$ and $4f_{5/2}$ lines are 4.87 eV. The peak maxima of the Pb $4f_{7/2}$ core levels of $(BdA)PbI_4$, $(HdA)PbI_4$, and $(OdA)PbI_4$ are at a binding energy of 138.4 138.1, and 138.3 eV, respectively. The binding energy is similar to that of $(CH_3NH_3)PbI_3$ indicative of a Pb^{2+} oxidation state.[38] In previous investigations, similar samples have exhibited spectral features indicating the presence of metallic lead (Pb^0), negatively impacting the performance by providing nonradiative decay pathways.[38-40] However, no signature of Pb^0 was found for the samples investigated here, which suggests there was proper crystallization during synthesis and enhanced stability to the reduction of lead. It should be noted that metallic lead features are a directly related to synthesis and annealing conditions.[38] Figure 1c shows a single I $3d_{5/2}$ core level at a binding energies of 619.2, 618.9, and 619.1 eV for $(BdA)PbI_4$, $(HdA)PbI_4$, and $(OdA)PbI_4$ samples respectively. The spin−orbit splitting between I $3d_{5/2}$ and I $3d_{3/2}$ is 11.5 eV for all samples. The binding energy separation between the Pb 4*f* and I 3*d* core levels is found to be the same in all samples, and also very similar to what has previously been found for $(CH_3NH_3)PbI_3$[39], (Table S1). This indicates that lead and iodide are in the same oxidation states (Pb^{2+} and I^-) for the entire series and that iodine and lead have similar local electronic environments in all compounds. In light of the constant binding energy difference between Pb 4*f* and I 3*d* as well as with N 1*s* and C 1*s* (Figure 1d), we observe that the differences in core level binding energy positions is largely the result of the position of the Fermi level in the bandgap.

3.1 VALENCE BAND

The valence band spectra of the 2D perovskites on mesoporous-TiO_2 ($mTiO_2$) are presented in Figure 2 along with the precursor PbI_2 for comparison. The overall spectral contributions to the valence band are quite similar, with the exception of the band edge positions towards lower binding energy. At

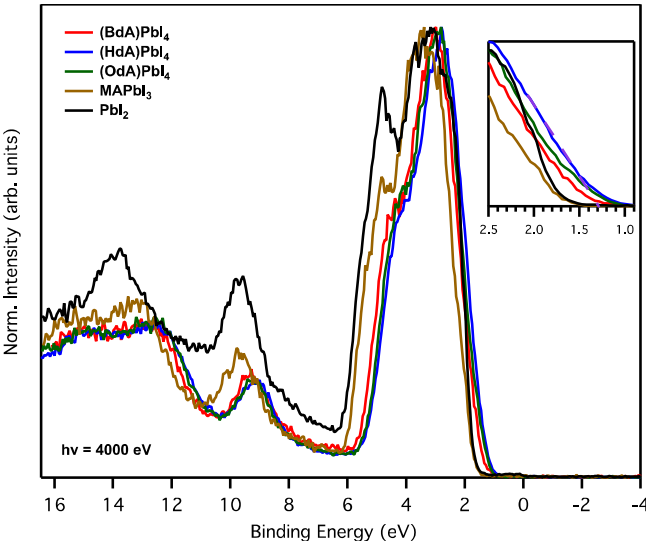

Figure 2. HAXPES spectra of the valence bands for the 2D perovskites ($BdAPbI_4$, $HdAPbI_4$, and $OdAPbI_4$), along with the 3D $MAPbI_3$ and the precursor PbI_2. The inset shows the extrapolated line used to determine the valence band maximum.

the photon energies used here, the probe depth (defined as three times the inelastic mean free path) can be estimated to 10 nm, indicating that the signal is dominating from structures below the surface atomic layers and should be less affected by possibly surface reconstruction or dangling bonds. The spectral contributions from 1.75 – 5 eV for the 2D perovskites in Figure 2 originates from levels with iodine and lead character, as discussed later. The inset in Figure 2, the abscissa (purple dashed line) of the trailing edge is used to approximate the VB offset from the Fermi level (E_F). The intersections for VB offset are listed in Table S2. The VB offsets from the Fermi level (set to 0 eV of Au Fermi level) all fall within 250 meV for the considered samples. The relative difference between the core level signals for the 2D HOP are nearly the same, and therefore the shift in the valence band maximum is a result of a Fermi level shift. The valence band position for $(HdA)PbI_4$ is the closest in the 2D HOP series to the Fermi energy, which indicates that this material is the most capable to oxidize in the 2D series. This is in agreement with previous electrochemical studies on these materials.[21]

The calculated total and partial DOS in the valence band is presented in Figure 3. The results of the calculated DOS and experimental VB (Figure 2) are in reasonable agreement indicating similar band edge profile for the three samples. The partial density of states due to carbon and nitrogen moieties are found between 8 and 13 eV, as reported previously for similar organic-inorganic perovskites[38, 39, 41] At the excitation energies used in our experiments, the corresponding spectral features are very weak due to the small photoionization cross sections for carbon and nitrogen in comparison to lead and iodine. The spectral features characteristic of the precursor PbI_2 and 3D $MAPbI_3$ at ≈ 5 eV, 10 eV, and 14 eV are similar to that of 2D perovskites. Near the valence band edge, the electronic contribution originates solely from the inorganic sheets for the HOPs and PbI_2. However, there is a noticeable change in the valence band for our 2D materials. The elemental contribution to the upper edge (~ 5 eV) of the valence band of our samples and PbI_2 show similar hybridization between I 5*p* and Pb 6*s*, while the bandwidth for all 2D HOP samples are much narrower than to that of layered PbI2 and

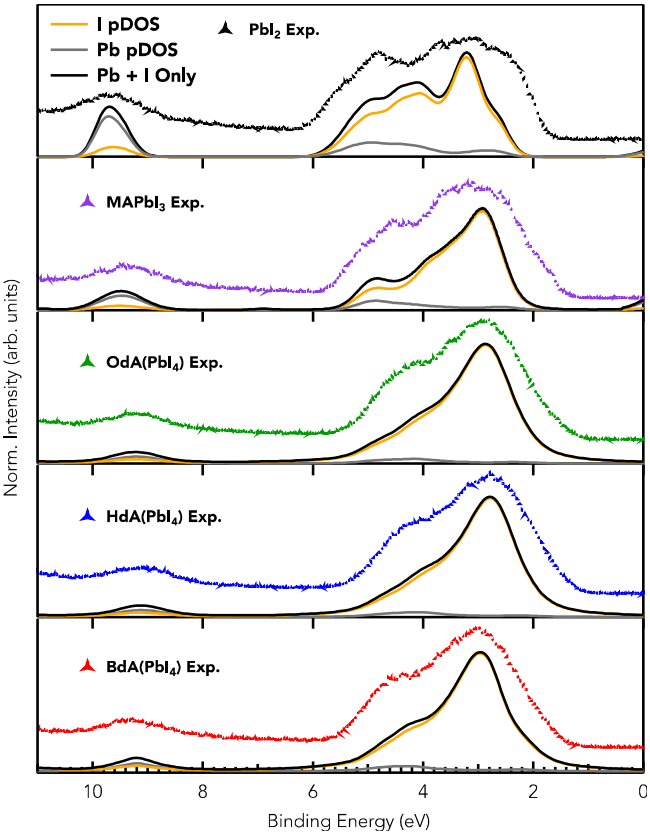

Figure 3. The calculated valence band spectra are presented with respect to the experimental spectra. Calculations are divided into individual atomic contributions to the valence band.

the 3D $MAPbI_3$. This is an indication that the organic cation-linked 2D perovskites constitute more localized bands than the layered PbI_2 and $MAPbI_3$ counterpart. This outcome is also consistent with the lower dimensionality of the layered HOPs.[42] Since the same spectral features exist for PbI_2 and $MAPbI_3$ and the 2D perovskite samples, with the same orbital contributions at the edge of the valence band, the relative position of the band edge can be attributed to modification in the bandwidth of the orbitals and the Fermi level position in the 2D monolayer samples. In order to determine iodine's role and modification in the frontier states, we exploit the element specific nature of HERFD-XANES and RIXS to probe occupied and unoccupied orbitals of iodine.

3.2 HERFD-XANES & RIXS

Figure 4 shows the experimental XANES spectra (Fig. 4a) and RIXS spectra (Fig. 4b) for the same set of samples. The XANES spectra show the unoccupied *p* states of iodine and follow dipole allowed transitions. The 2D HOP samples have some differences in local symmetry and coordination that are reflected in the differences in the absorption spectrum. The position of the absorption edge near 5,188 eV (*inset Fig. 4a*, determined by maximum of second derivative) for the different samples indicates slightly different conduction band positions. This is observed from $(BdA)PbI_4$ to $(HdA)PbI_4$ and is in a similar sequence to the onset of absorption from UV-vis spectra. An increase in intensity implies a larger number of unoccupied states for $(BdA)PbI_4$ at regions marked *I* and *II* in the spectra. This increase may be the consequence of lower symmetry compared with $(HdA)PbI_4$ and $(OdA)PbI_4$, which is

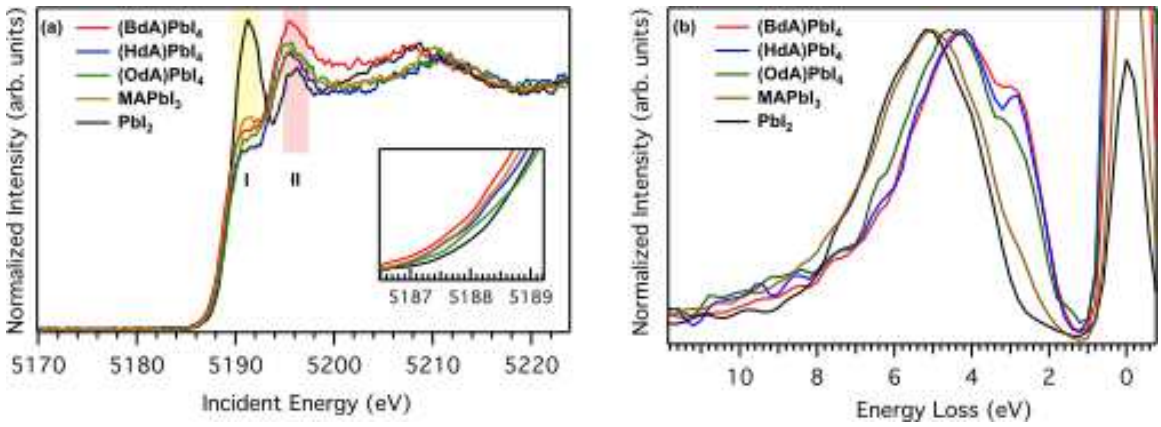

Figure 4. (a) Spectra of unoccupied states of iodine obtained by HERFD-XANES, and the inset shows the rising edge of the absorption spectrum and b. Occupied states of iodine in the three 2D perovskite samples (along with reference $MAPbI_3$ and PbI_2) obtained from RIXS plotted on an energy loss axis.

seen by minor changes to lattice positions as well as octahedral tilt. For PbI_2, the intensity in the highlighted region is the likely result of stronger I-Pb-I chemical bonding by virtue of shorter distances between adjacent lead atoms. The higher energy region shows narrower features of likely 6*p* states. The signature differences from $MAPbI_3$ and PbI_2 versus our separate 2D layered compounds are the broadening of the unoccupied *p* orbitals and a change in the available states in the conduction band for the 2D HOP materials.

RIXS spectra, taken at the first maximum of iodine L_1 absorption edge at an incident energy of 5190 eV, are shown in Figure 4b. The main structures are attributed to the transition from I 5*p* to I 2*s* orbitals, i.e. the $L\gamma_4$ emission line. The spectra represent the distribution of I 5*p* DOS in the valence band of the studied compounds. A comparison of the spectra of $(BdA)PbI_4$, $(HdA)PbI_4$, and $(OdA)PbI_4$ with those of $MAPbI_3$ and PbI_2 on the energy loss scale reveals the I 5*p* behavior similar to that detected in the HAXPES spectra of the valence band in Fig. 3, i.e. a significant amount of the spectral weight appears at the higher energy loss in $MAPbI_3$ and PbI_2. However, the RIXS spectra can be more affected by the transition matrix elements compared to the photoemission spectra. This is usually reflected in a reduced contribution of the DOS at the bottom of the valence band to the RIXS spectra, thus enhancing the relative contribution of the states at the top of the valence band to these spectra.

The above discussed increase in the spectral weight at the higher energy loss while going from $(BdA)PbI_4$, $(HdA)PbI_4$ and $(OdA)PbI_4$ to PbI_2 is in agreement with the DFT-predicted changes in the occupied I 5*p* DOS reported below for these compounds and which originate from the weaker I 5*p* – Pb 6*s*,*p* hybridization in PbI_2 due to larger I-Pb distances. An interesting feature of the RIXS spectra of the 2D compounds is a presence of the structure/shoulder at the energy loss of around 2.5 eV. This structure is seen for all three 2D materials while the DFT calculations predict such a distinct structure only for $(BdA)PbI_4$. This structure is a result of the I 5*p* – Pb 6*s* hybridization and originates from the 5*p* orbitals of so-called axial I atoms pointing towards the Pb atoms (see supporting information Figure S2). The valence edge states of iodine *5p* also has a shift towards lower energy loss for $(BdA)PbI_4$ followed by $(HdA)PbI_4$ and $(OdA)PbI_4$. This trend follows the sequence of increasing band gap from $(BdA)PbI_4$ (2.37 eV), $(HdA)PbI_4$ (2.44 eV), and $(OdA)PbI_4$ (2.55 eV) and is in agreement with the photoemission spectra reported earlier. This leads us to conclude that the effects by forming layered 2D perovskites with a large cation, as a result of the lower dimensionality, modify the position of the iodine orbitals at the edge of the valence band.

In Figure 5, schematic diagram of the relative band positions of the materials are presented. The position of the valence band maximum (VBM) has been determined from HAXPES data and the position of the conduction band minimum (CBM) relative to E_F is estimated by subtracting the optical band gap from the VBM. From this picture, we observe limited changes at the conduction band minimum, as seen in the Iodine L_1 absorption spectrum. From the relative positions of the CBM, electron transfer at the interface is energetically favorable. This finding can suggest our materials can be employed in several different charge extraction devices, and would be most suitable for a tandem solar cell.

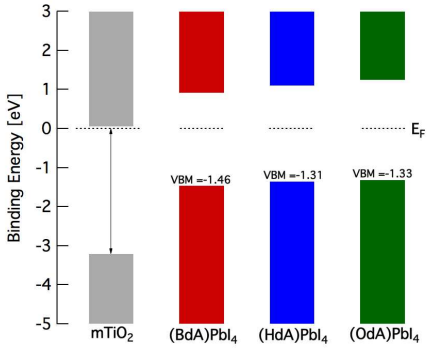

Figure 5. Energy band diagram of the 2D perovskite materials highlighting the differences in the valence band maximum position. Recorded data from HAXPES have been used alongside optical band gap data from the previous report.[21]

3.3 DFT CALCULATIONS

The total DOS and PDOS for the 2D lead perovskites as well as layered PbI_2 and the 3D $MAPbI_3$ are presented in Figure 6. The organic cation states do not directly participate in the states close to the VB or CB edges;, but indirectly affect the bandgap through the structural changes imposed in the inorganic structure[43] of the perovskite lattice. The plot high

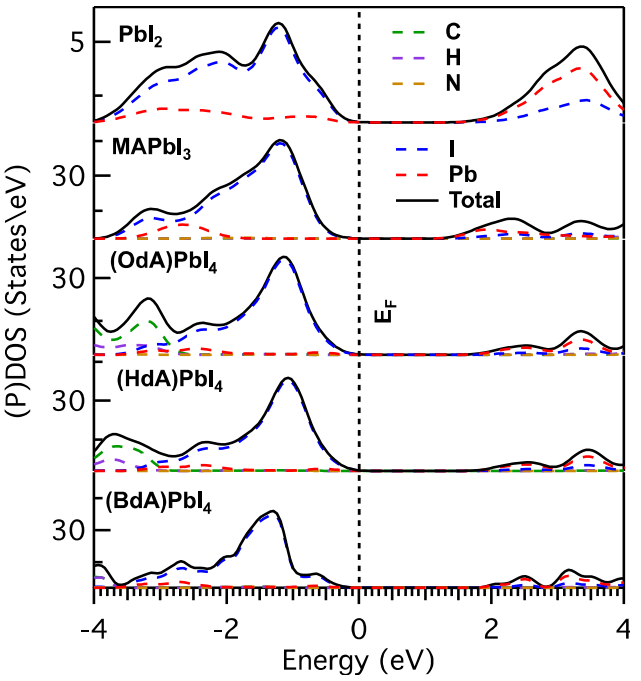

Figure 6. Calculated total and partial density of states (DOS) of 2D perovskites plotted alongside PbI_2 and 3D $MAPbI_3$. Partial density of states (PDOS) show a dominating orbital contribution from iodine in the valence band and lead orbitals in the conduction band for the 2D and 3D perovskites, and a slight contribution of iodine in the CB of PbI_2. The 2D perovskites with the shortest alkyl chain ($BdAPbI_4$) show distortion of the valence band edge, consistent with the increased inter-layer interaction. The Fermi level has been set to 0 eV.

-lights the contribution of the lead 6*s* and iodide 5*p* orbitals in the VB and CB edges and is in agreement with our experimental HAXPES valence band and I XANES and RIXS.[31] All of the 2D structures have a nearly similar direct band gap close to 2.14 eV from the theoretical calculations. The experimental band gaps, however, display a difference of 0.35 eV in comparison to calculated values. Considering the DFT error for band gap estimation and neglecting excitonic effects, this difference is reasonable. For bulk $MAPbI_3$, an error cancelation coming from neglecting SOC effects[34] is also expected. The magnitude of these effects are so far not known for 2D perovskites since inclusion of GW or hybrid DFT and van der Waals interaction would alter the picture in addition to SOC effects. Quantum confinement effects can also be responsible for band narrowing and slight band edge shifts in 2D layered perovskites and is partly included in the DFT calculations. However, due to the strong columbic hole-electron interactions, this effect cannot be well described within a DFT framework based on local density approximation (LDA) or general gradient approximation (GGA) functionals.

The band structures were calculated for all of the 2D perovskite for different directions within the first Brillouin zone are presented in Figure 7. The second derivative of the band edges versus energy for 2D HOPs are rather small compared to the 3D crystal at the optical transition point Γ, and therefore a larger effective mass for charge carriers. One can also observe a directional dependence for the effective masses (see Fig. 7); the charge carrier effective masses are smaller for the in-plane directions within the inorganic planes and are much larger perpendicular to the inorganic plane, *i.e.* a direction between

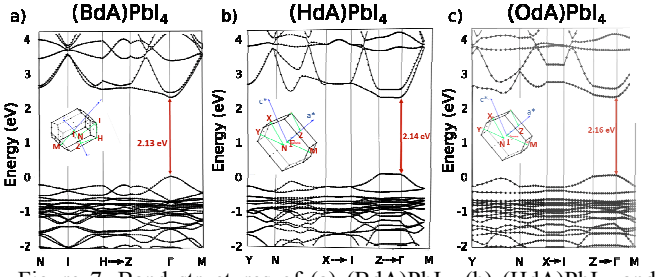

Figure 7. Band structures of (a) $(BdA)PbI_4$, (b) $(HdA)PbI_4$, and (c) $(OdA)PbI_4$ together with K-space paths with the first Brillouin zone and their estimated band-gap values calculated with DFT.

two inorganic planes separated by the organic molecules. This is in line with the expectation that the charge transport mainly occurs within the inorganic network. In addition, a dispersion for the direction perpendicular to the inorganic network is observed for the shortest alkyl chain $(BdA)PbI_4$ perovskite (Fig. 7a), showing an interaction and possible charge transport in between the layers. This dispersion becomes flatter for $(HdA)PbI_4$ and disappears for the $(OdA)PbI_4$ (Fig. 7c). Therefore the observed distant dependence can be interpreted as long range columbic interactions between the interlayers revealing that for distances longer than 6 Å limit, there is no interaction between the inorganic planes. A charge density plot between two closest inorganic interlayers (Fig. S3) also support this showing that there is more charge density in between the two nearest iodine atoms for shorter alkyl chain 2D perovskite compared to the larger alkyl chain 2D perovskite which in agreement with band structure dispersions observed for Γ to Z direction (Fig. 7).

By analyzing the bond lengths and angles of the three 2D perovskite (see Table S3), we found more variation in the lead-iodide bond lengths and angles for $(BdA)PbI_4$ as compared with $(HdA)PbI_4$ and $(OdA)PbI_4$. The in-plane Pb-I-Pb angle of the adjacent octahedra deviates substantially from the $MAPbI_3$ cubic structure (180˚) for $(BdA)PbI_4$ (see Fig. 7). This observed variation show that the main structural and composition differences between the samples are the lengths of the organic cations and suggests that for $(BdA)PbI_4$, different bonding orbitals are more equal in energy and thus allow a larger variation in bond length. A longer organic cation has previously reported to induce a blue shift in the band gap[44] but also includes effects of distortion of the curvature of inorganic Pb-I layer and thus variation in Pb-I bond lengths and angles, something not included in our DFT calculations where we instead see only a slight modification in the charge density profile within the unit cell (plots of the 2D perovskites within the inorganic plane depicted in Fig. S3).

3.4 Pb and I UNIT CELL DENSITY

Based on previously reported crystallographic data for these 2D perovskite materials[21] and 3D $(CH_3NH_3)PbI_3$[15], we have calculated Pb and I number density (per volume) in the unit cells (Table 2). The results are presented in Table 2. By introducing a bulkier cation in the unit cell for 2D perovskite, the volume of unit cell increases compared to 3D perovskite [cf. $(CH_3NH_3)PbI_3$], which leads to a reduced number of lead and iodide atoms per volume for 2D perovskites. We can assume that the extinction coefficients for the 2D perovskite materials to be proportional to Pb and I atom number densities since the optical transition is in between the electronic states belonging to lead and iodide. It was proposed for methylammonium lead iodide[45, 46] that the organic cation is not contributing in the

visible light absorption, but can indirectly affect the properties by induced perturbation of the inorganic lattice. Based on the reduction of Pb and I atom number density from 3D to 2D and following the 2D series with the bulkier cation from $(BdA)PbI_4$ to $(OdA)PbI_4$, a decreasing trend in the absorption coefficient and light harvesting efficiency can be expected from our data (Table 2) which also is in agreement with corresponding experimental UV-visible spectra of these materials.[15, 21]

Table 2. Calculated lead and iodide density per unit cell volume based on the single crystallographic data. [15, 21]

	Pb density / $(nm)^{-3}$	I density / $(nm)^{-3}$
3D– $(CH_3NH_3)PbI_3$	4.03	12.09
2D – $(BdA)PbI_4$	2.61	10.45
2D– $(HdA)PbI_4$	2.32	9.29
2D– $(OdA)PbI_4$	2.02	8.09

An early report on $CH_3NH_3PbI_3$ perovskite predicted an extinction coefficient of 1.6×10^4 $M^{-1}cm^{-1}$ at 490 nm.[47] Following this and the assumption of no contribution from the orbitals of the organic cations in light absorption (apart from the perturbation of the inorganic lattice), approximate theoretical extinction coefficient of 1.0, 0.9, and 0.8×10^4 $M^{-1}cm^{-1}$ can be estimated for $(BdA)PbI_4$, $(HdA)PbI_4$, and $(OdA)PbI_4$ respectively. The change in electron density is also experimentally observed in the XANES and RIXS spectra of the 2D hybrid perovskites compared to PbI_2; from XANES there is a decrease in intensity at section I for the 2D perovskites relative to PbI_2 and from RIXS there is an increase in intensity at low energy relative to PbI_2. The calculations of DOS and PDOS support this picture and show similar effects for an increase in valence band density and decrease in conduction band density.

4. CONCLUSION

We have presented a detailed experimental and theoretical investigation of three different 2D perovskite solar cell materials with varying inter-layer distance and compared with PbI_2 and $MAPbI_3$. The electronic structure of the valence band and conduction band for these materials was investigated by HAXPES, XANES, and RIXS. In contrast to the layered PbI_2, the observed structural changes in the 2D hybrid materials results in a dimensional constraint of the inorganic layer. The results show similar spectral weight to the partial density of states with different degree of hybridization between the I 5*p* and Pb 6*s* orbitals but a noticeable narrowing of the states at the edge of the valence and conduction bands. A key distinction in the materials studied from spectroscopic data is the positions of the Fermi level. The interface energetics from HAXPES data show a band interface that is suitable for electron injection into a $mTiO_2$ substrate. Our spectra show that only slight changes to the overall electronic structure result from varying the inorganic interlayer distance if effects of bending and bond-length variations are held to a minimal. This picture is supported by DFT band structure calculations which also show a clear directional dependence changes in the dispersion at band edges, in agreement with suggested in-plane directional carrier transport. Effective mass of electrons and holes for the interlayer charge transport show a dependency on the alkyl chain lengths and thus the distance between the inorganic layers. By analyzing the near band edge dispersions, i.e. more energy dispersion in $(BdA)PbI_4$ and no dispersion in the $(OdA)PbI_4$ system, we could estimate a cut-off of the columbic interaction distance of about 6 Å after which there is minor or no interaction between the inorganic layers. Since the layered 2D perovskite has recently shown great advancement in terms of efficiency and stability of solar cells,[48] the present findings can reveal key parameters for increased control of band alignments for matching energy levels and charge carrier mobilities toward more efficient 2D perovskite devices.

ASSOCIATED CONTENT

Supporting Information

The Supporting Information is available free of charge on the ACS Publications website.

A figure that shows shallow core levels used to determine material stoichiometry between lead and iodine. A table that lists the binding energy separation between iodine and lead core-level peaks, and valence band offsets from HAXPES data. A calculated projected density of states that shows contribution from axial and equatorial iodine atoms. Charge density plots and bond lengths between lead and iodine atoms for the 2D HOP. (PDF)

AUTHOR INFORMATION

Corresponding Author

* (James M. Gardner) E-mail: jgardner@kth.se
* (Håkan Rensmo) E-mail: hakan.rensmo@physics.uu.se

Author Contributions

The manuscript was written through contributions of all authors. / All authors have given approval to the final version of the manuscript. ‡These authors contributed equally.

Funding Sources

This work was supported by Swedish Government through "STandUP for ENERGY", The Swedish Energy Agency, The Swedish Research Council, Knut & Alice Wallenberg Foundation.

Notes

The authors declare no competing financial interest.

ACKNOWLEDGMENT

We acknowledge HZB and ESRF for the allocation of synchrotron radiation beamtime. We acknowledge Uppsala Multidisciplinary Center for Advanced Computational Science (UPPMAX) for providing the computational resources under Project 2017-1-158.

REFERENCES

(1) Dieter, W. CH3NH3PbX3, ein Pb(II)–system mit kubischer perowskitstruktur. *Zeitschrift für Naturforschung B* **1978,** 33, 1443–1445.

(2) Poglitsch, A.; Weber, D., Dynamic disorder in methylammoniumtrihalogenoplumbates (II) observed by millimeter□wave spectroscopy. *The Journal of Chemical Physics* **1987,** 87, (11), 6373-6378.

(3) Kojima, A.; Teshima, K.; Shirai, Y.; Miyasaka, T., Organometal Halide Perovskites as Visible-Light Sensitizers for Photovoltaic

Cells. *Journal of the American Chemical Society* **2009,** 131, (17), 6050-6051.

(4) NREL Chart. https://www.nrel.gov/pv/assets/images/efficiency-chart.png (accessed January 17, 2018).

(5) Kim, H.-S.; Lee, C.-R.; Im, J.-H.; Lee, K.-B.; Moehl, T.; Marchioro, A.; Moon, S.-J.; Humphry-Baker, R.; Yum, J.-H.; Moser, J. E.; Gratzel, M.; Park, N.-G., Lead Iodide Perovskite Sensitized All-Solid-State Submicron Thin Film Mesoscopic Solar Cell with Efficiency Exceeding 9%. *Sci. Rep.* **2012,** 2.

(6) Lee, M. M.; Teuscher, J.; Miyasaka, T.; Murakami, T. N.; Snaith, H. J., Efficient Hybrid Solar Cells Based on Meso-Superstructured Organometal Halide Perovskites. *Science* **2012,** 338, (6107), 643-647.

(7) Burschka, J.; Pellet, N.; Moon, S.-J.; Humphry-Baker, R.; Gao, P.; Nazeeruddin, M. K.; Gratzel, M., Sequential deposition as a route to high-performance perovskite-sensitized solar cells. *Nature* **2013,** 499, (7458), 316-319.

(8) Liu, M.; Johnston, M. B.; Snaith, H. J., Efficient planar heterojunction perovskite solar cells by vapour deposition. *Nature* **2013,** 501, (7467), 395-398.

(9) Jeon, N. J.; Noh, J. H.; Kim, Y. C.; Yang, W. S.; Ryu, S.; Seok, S. I., Solvent engineering for high-performance inorganic–organic hybrid perovskite solar cells. *Nature Materials* **2014,** 13, (9), 897-903.

(10) Yang, W. S.; Noh, J. H.; Jeon, N. J.; Kim, Y. C.; Ryu, S.; Seo, J.; Seok, S. I., High-performance photovoltaic perovskite layers fabricated through intramolecular exchange. *Science* **2015,** 348, (6240), 1234-1237.

(11) Baikie, T.; Fang, Y.; Kadro, J. M.; Schreyer, M.; Wei, F.; Mhaisalkar, S. G.; Graetzel, M.; White, T. J., Synthesis and crystal chemistry of the hybrid perovskite (CH3NH3)PbI3 for solid-state sensitised solar cell applications. *Journal of Materials Chemistry A* **2013,** 1, (18), 5628-5641.

(12) Pathak, S.; Sepe, A.; Sadhanala, A.; Deschler, F.; Haghighirad, A.; Sakai, N.; Goedel, K. C.; Stranks, S. D.; Noel, N.; Price, M.; Hüttner, S.; Hawkins, N. A.; Friend, R. H.; Steiner, U.; Snaith, H. J., Atmospheric Influence upon Crystallization and Electronic Disorder and Its Impact on the Photophysical Properties of Organic–Inorganic Perovskite Solar Cells. *ACS Nano* **2015,** 9, (3), 2311-2320.

(13) Yang, J.; Siempelkamp, B. D.; Mosconi, E.; De Angelis, F.; Kelly, T. L., Origin of the Thermal Instability in CH3NH3PbI3 Thin Films Deposited on ZnO. *Chemistry of Materials* **2015,** 27, (12), 4229-4236.

(14) Misra, R. K.; Aharon, S.; Li, B.; Mogilyansky, D.; Visoly-Fisher, I.; Etgar, L.; Katz, E. A., Temperature- and Component-Dependent Degradation of Perovskite Photovoltaic Materials under Concentrated Sunlight. *The Journal of Physical Chemistry Letters* **2015,** 6, (3), 326-330.

(15) Safdari, M.; Fischer, A.; Xu, B.; Kloo, L.; Gardner, J. M., Structure and function relationships in alkylammonium lead(ii) iodide solar cells. *Journal of Materials Chemistry A* **2015,** 3, (17), 9201-9207.

(16) Smith, I. C.; Hoke, E. T.; Solis-Ibarra, D.; McGehee, M. D.; Karunadasa, H. I., A Layered Hybrid Perovskite Solar-Cell Absorber with Enhanced Moisture Stability. *Angewandte Chemie International Edition* **2014,** 53, (42), 11232-11235.

(17) Cao, D. H.; Stoumpos, C. C.; Farha, O. K.; Hupp, J. T.; Kanatzidis, M. G., 2D Homologous Perovskites as Light-Absorbing Materials for Solar Cell Applications. *Journal of the American Chemical Society* **2015,** 137, (24), 7843-7850.

(18) Stoumpos, C. C.; Cao, D. H.; Clark, D. J.; Young, J.; Rondinelli, J. M.; Jang, J. I.; Hupp, J. T.; Kanatzidis, M. G., Ruddlesden–Popper Hybrid Lead Iodide Perovskite 2D Homologous Semiconductors. *Chemistry of Materials* **2016,** 28, (8), 2852-2867.

(19) Wang, Z.; Lin, Q.; Chmiel, F. P.; Sakai, N.; Herz, L. M.; Snaith, H. J., Efficient ambient-air-stable solar cells with 2D–3D heterostructured butylammonium-caesium-formamidinium lead halide perovskites. *Nature Energy* **2017,** 2, 17135-17139.

(20) Grancini, G.; Roldán-Carmona, C.; Zimmermann, I.; Mosconi, E.; Lee, X.; Martineau, D.; Narbey, S.; Oswald, F.; De Angelis, F.; Graetzel, M., One-Year stable perovskite solar cells by 2D/3D interface engineering. *Nat. Commun.* **2017,** 8, 1-8.

(21) Safdari, M.; Svensson, P. H.; Hoang, M. T.; Oh, I.; Kloo, L.; Gardner, J. M., Layered 2D alkyldiammonium lead iodide perovskites: synthesis, characterization, and use in solar cells. *Journal of Materials Chemistry A* **2016,** 4, (40), 15638-15646.

(22) de Groot, F., High-Resolution X-ray Emission and X-ray Absorption Spectroscopy. *Chemical Reviews* **2001,** 101, (6), 1779-1808.

(23) Mitzi, D.; Wang, S.; Feild, C.; Chess, C.; Guloy, A., Conducting layered organic-inorganic halides containing (110)-oriented perovskite sheets. *Science* **1995,** 267, (5203), 1473.

(24) Walsh, A., Principles of Chemical Bonding and Band Gap Engineering in Hybrid Organic–Inorganic Halide Perovskites. *The Journal of Physical Chemistry C* **2015,** 119, (11), 5755-5760.

(25) Gorgoi, M.; Svensson, S.; Schäfers, F.; Öhrwall, G.; Mertin, M.; Bressler, P.; Karis, O.; Siegbahn, H.; Sandell, A.; Rensmo, H.; Doherty, W.; Jung, C.; Braun, W.; Eberhardt, W., The high kinetic energy photoelectron spectroscopy facility at BESSY progress and first results. *Nuclear Instruments and Methods in Physics Research Section A: Accelerators, Spectrometers, Detectors and Associated Equipment* **2009,** 601, (1–2), 48-53.

(26) Scofield, J., *Electron Spectrosc. Relat. Phenom.* **1976,** 8.

(27) Gauthier, C.; Sole, V. A.; Signorato, R.; Goulon, J.; Moguiline, E., The ESRF beamline ID26: X-ray absorption on ultra dilute sample. *Journal of Synchrotron Radiation* **1999,** 6, (3), 164-166.

(28) Atkins, A. J.; Jacob, C. R.; Bauer, M., Probing the Electronic Structure of Substituted Ferrocenes with High-Resolution XANES Spectroscopy. *Chemistry – A European Journal* **2012,** 18, (23), 7021-7025.

(29) Giannozzi, P.; Baroni, S.; Bonini, N.; Calandra, M.; Car, R.; Cavazzoni, C.; Ceresoli, D.; Chiarotti, G. L.; Cococcioni, M.; Dabo, I., QUANTUM ESPRESSO: a modular and open-source software project for quantum simulations of materials. *Journal of physics: Condensed matter* **2009,** 21, (39), 395502.

(30) Dovesi, R.; Orlando, R.; Civalleri, B.; Roetti, C.; Saunders, V. R.; Zicovich-Wilson, C. M., CRYSTAL: a computational tool for the ab initio study of the electronic properties of crystals. *Zeitschrift für Kristallographie* **2005,** 220, (5/6), 571–573.

(31) Pazoki, M.; Jacobsson, T. J.; Hagfeldt, A.; Boschloo, G.; Edvinsson, T., Effect of metal cation replacement on the electronic structure of metalorganic halide perovskites: Replacement of lead with alkaline-earth metals. *Physical Review B* **2016,** 93, (14), 144105.

(32) Jacobsson, T. J.; Pazoki, M.; Hagfeldt, A.; Edvinsson, T., Goldschmidt's rules and strontium replacement in lead halogen perovskite solar cells: Theory and preliminary experiments on CH3NH3SrI3. *The Journal of Physical Chemistry C* **2015,** 119, (46), 25673-25683.

(33) Perdew, J. P.; Chevary, J. A.; Vosko, S. H.; Jackson, K. A.; Pederson, M. R.; Singh, D. J.; Fiolhais, C., Atoms, molecules, solids, and surfaces: Applications of the generalized gradient approximation for exchange and correlation. *Physical Review B* **1992,** 46, (11), 6671-6687.

(34) Umari, P.; Mosconi, E.; De Angelis, F., Relativistic GW calculations on CH3NH3PbI3 and CH3NH3SnI3 Perovskites for Solar Cell Applications. *Scientific Reports* **2014,** 4, 4467.

(35) Pazoki, M.; Johansson, M. B.; Zhu, H.; Broqvist, P.; Edvinsson, T.; Boschloo, G.; Johansson, E. M., Bismuth Iodide Perovskite Materials for Solar Cell Applications: Electronic Structure, Optical Transitions, and Directional Charge Transport. *The Journal of Physical Chemistry C* **2016,** 120, (51), 29039-29046.

(36) Safdari, M.; Svensson, P. H.; Hoang, M. T.; Oh, I.; Kloo, L.; Gardner, J. M., Layered 2D Alkyldiammonium Lead Iodide Perovskites: Synthesis, Characterization, and Use in Solar Cells. *Journal of Materials Chemistry A* **2016**, 4, 15638-15646.

(37) Kokalj, A., Computer graphics and graphical user interfaces as tools in simulations of matter at the atomic scale. *Computational Materials Science* **2003,** 28, (2), 155-168.

(38) Lindblad, R.; Jena, N. K.; Philippe, B.; Oscarsson, J.; Bi, D.; Lindblad, A.; Mandal, S.; Pal, B.; Sarma, D. D.; Karis, O.; Siegbahn, H.; Johansson, E. M. J.; Odelius, M.; Rensmo, H., Electronic Structure of CH3NH3PbX3 Perovskites: Dependence on the Halide Moiety. *The Journal of Physical Chemistry C* **2015,** 119, (4), 1818-1825.

(39) Lindblad, R.; Bi, D.; Park, B.-w.; Oscarsson, J.; Gorgoi, M.; Siegbahn, H.; Odelius, M.; Johansson, E. M. J.; Rensmo, H., Electronic Structure of TiO2/CH3NH3PbI3 Perovskite Solar Cell Interfaces. *The Journal of Physical Chemistry Letters* **2014,** 5, (4), 648-653.

(40) Sadoughi, G.; Starr, D. E.; Handick, E.; Stranks, S. D.; Gorgoi, M.; Wilks, R. G.; Bär, M.; Snaith, H. J., Observation and Mediation of the Presence of Metallic Lead in Organic–Inorganic Perovskite Films. *ACS applied materials & interfaces* **2015,** 7, (24), 13440-13444.

(41) Philippe, B.; Jacobsson, T. J.; Correa-Baena, J.-P.; Jena, N. K.; Banerjee, A.; Chakraborty, S.; Cappel, U. B.; Ahuja, R.; Hagfeldt, A.; Odelius, M., Valence Level Character in a Mixed Perovskite Material and Determination of the Valence Band Maximum from Photoelectron Spectroscopy: Variation with Photon Energy. *The Journal of Physical Chemistry C* **2017,** 121, (48), 26655-26666.

(42) Kamminga, M. E.; Fang, H.-H.; Filip, M. R.; Giustino, F.; Baas, J.; Blake, G. R.; Loi, M. A.; Palstra, T. T. M., Confinement Effects in Low-Dimensional Lead Iodide Perovskite Hybrids. *Chemistry of Materials* **2016,** 28, (13), 4554-4562.

(43) Filip, M. R.; Eperon, G. E.; Snaith, H. J.; Giustino, F., Steric engineering of metal-halide perovskites with tunable optical band gaps. *Nat. Commun.* **2014**, 5, 5757.

(44) Kamminga, M. E.; Fang, H.-H.; Filip, M. R.; Giustino, F.; Baas, J.; Blake, G. R.; Loi, M. A.; Palstra, T. T., Confinement effects in low-dimensional lead iodide perovskite hybrids. *Chemistry of Materials* **2016,** 28, (13), 4554-4562.

(45) Wang, Y.; Gould, T.; Dobson, J. F.; Zhang, H.; Yang, H.; Yao, X.; Zhao, H., Density functional theory analysis of structural and electronic properties of orthorhombic perovskite CH3NH3PbI3. *Physical Chemistry Chemical Physics* **2014,** 16, (4), 1424-1429.

(46) Buin, A.; Comin, R.; Xu, J.; Ip, A. H.; Sargent, E. H., Halide-Dependent Electronic Structure of Organolead Perovskite Materials. *Chemistry of Materials* **2015,** 27, (12), 4405-4412.

(47) Im, J.-H.; Lee, C.-R.; Lee, J.-W.; Park, S.-W.; Park, N.-G., 6.5% efficient perovskite quantum-dot-sensitized solar cell. *Nanoscale* **2011,** 3, (10), 4088-4093.

(48) Tsai, H.; Nie, W.; Blancon, J.-C.; Stoumpos, C. C.; Asadpour, R.; Harutyunyan, B.; Neukirch, A. J.; Verduzco, R.; Crochet, J. J.; Tretiak, S.; Pedesseau, L.; Even, J.; Alam, M. A.; Gupta, G.; Lou, J.; Ajayan, P. M.; Bedzyk, M. J.; Kanatzidis, M. G.; Mohite, A. D., High-efficiency two-dimensional Ruddlesden–Popper perovskite solar cells. *Nature* **2016,** 536, 312-316.

Authors are required to submit a graphic entry for the Table of Contents (TOC) that, in conjunction with the manuscript title, should give the reader a representative idea of one of the following: A key structure, reaction, equation, concept, or theorem, etc., that is discussed in the manuscript. Consult the journal's Instructions for Authors for TOC graphic specifications.